Conductance and Permeability of the Residual State of Connexin43 Gap Junction Channels

Feliksas F. Bukauskas, Angele Bukauskiene, and Vytas K. Verselis

Department of Neuroscience, Albert Einstein College of Medicine, Bronx, NY 10461

ABSTRACT We used cell lines expressing wild-type connexin43 and connexin43 fused with the enhanced green fluorescent protein (Cx43-EGFP) to examine conductance and perm-selectivity of the residual state of Cx43 homotypic and Cx43/Cx43-EGFP heterotypic gap junction channels. Each hemichannel in Cx43 cell–cell channel possesses two gates: a fast gate that closes channels to the residual state and a slow gate that fully closes channels; the transjunctional voltage (V_j) closes the fast gate in the hemichannel that is on the relatively negative side. Here, we demonstrate macroscopically and at the single-channel level that the I-V relationship of the residual state rectifies, exhibiting higher conductance at higher V_js that are negative on the side of gated hemichannel. The degree of rectification increases when Cl^- is replaced by Asp^- and decreases when K^+ is replaced by TEA^+. These data are consistent with an increased anionic selectivity of the residual state. The V_j-gated channel is not permeable to monovalent positively and negatively charged dyes, which are readily permeable through the fully open channel. These data indicate that a narrowing of the channel pore accompanies gating to the residual state. We suggest that the fast gate operates through a conformational change that introduces positive charge at the cytoplasmic vestibule of the gated hemichannel, thereby producing current rectification, increased anionic selectivity, and a narrowing of channel pore that is largely responsible for reducing channel conductance and restricting dye transfer. Consequently, the fast V_j-sensitive gating mechanism can serve as a selectivity filter, which allows electrical coupling but limits metabolic communication.

KEY WORDS: intercellular communication • dye transfer • EGFP • voltage gating • permeability

INTRODUCTION

Connexins (Cxs),* a large family of homologous membrane proteins, form gap junction (GJ) channels that provide a direct pathway for electrical and metabolic signaling between cells (Bennett et al., 1991; Elfgang et al., 1995). Each GJ channel is composed of two hemichannels that, in turn, are composed of six connexin subunits. Connexins are predicted to have four α helical transmembrane domains (TM1–TM4), intracellular NH_2 and COOH termini (NT and CT, respectively), two extracellular loops (E1 and E2), and a cytoplasmic loop (Unwin and Zampighi, 1980; Yeager and Nicholson, 1996; Yeager, 1998). Freeze fracture electron microscopy has shown that GJ channels cluster tightly into 2-D arrays or plaques (Revel and Karnovsky, 1967; Peracchia, 1977). In cells transfected with connexins that are fused with enhanced green fluorescent protein (EGFP), GJ plaques can be visualized in living cells by fluorescence microscopy (Jordan et al., 1999; Falk, 2000), and it was shown that only channels assembled into junctional plaques are functional (Bukauskas et al., 2000). In invertebrates, GJ channels are formed of innexins, another large family of integral membrane proteins, and it is predicted that they also have four transmembrane domains and oligomerize into hemichannels composed of six subunits. Despite a lack of primary sequence homology with connexins, innexins form GJ channels with surprisingly similar functional properties (Verselis et al., 1991; Bukauskas et al., 1992; Bukauskas and Weingart, 1994; Phelan and Starich, 2001).

Junctional conductance (g_j) of GJ channels formed from all connexins is sensitive to transjunctional voltage (V_j) the voltage difference between the cells. In homotypic junctions, formed by the docking of identical hemichannels, reductions in g_j with V_j are typically symmetric about a maximum at $V_j = 0$. In heterotypic junctions, where asymmetry is formed by the docking of hemichannels differing in connexin composition, asymmetry in gating about $V_j = 0$ usually results. It was proposed that each hemichannel in a formed GJ channel has its own V_j gate and, for each polarity of V_j, closure can be ascribed to one hemichannel (Harris et al., 1981). A distinct property of V_j gating is that g_j does not decline to zero with increasing V_j, leaving a residual conductance that varies from ~5 to 30% of its maximum depending on the connexin type (Werner et al., 1989; Willecke et al., 1991; Rook et al., 1992; Moreno et al., 1995;

Address correspondence to F. Bukauskas, 1300 Morris Park Avenue, Bronx, NY 10461. Fax: (718) 430-8944. E-mail: fbukausk@aecom.yu.edu

*Abbreviations used in this paper: CT, COOH termini; Cx, connexin; EGFP, enhanced green fluorescent protein; GJ, gap junction; g_j, junctional conductance; NT, NH_2 termini; PNP, Poisson-Nernst-Plank; v_j, transjunctional voltage.

White et al., 1995; Steiner and Ebihara, 1996; Revilla et al., 1999). Single-channel studies have shown that the residual g_j is explained by gating of GJ channels to a long-lived substate (Bukauskas and Weingart, 1994; Moreno et al., 1994). Weingart and Bukauskas (1993) termed this substate the "residual" state, and demonstrated it to be a property common to vertebrate and invertebrate GJs (Bukauskas et al., 1995). GJ channels can close completely as well (i.e., to a nonconducting state in response to V_j), but has been shown to occur by a different mechanism (Banach and Weingart, 2000; Bukauskas et al., 2001). Gating to the residual and closed states is not only distinguished by the degree of channel closure, but also by kinetics and we have termed these two mechanisms "fast" and "slow" V_j gating, respectively.

Bukauskas and Weingart (1994) proposed that the residual state represents the most closed conformation for the fast V_j gate. Depending on the connexin composition, this gate has been shown to close for either polarity of V_j so that some hemichannels will close on relative negativity and others on relative positivity on their cytoplasmic sides. Molecular studies have shown that charged residues in the NT domain form the voltage sensor for fast V_j gating and that the sign of the charge on the sensor confers gating polarity (Verselis et al., 1994; Oh et al., 2000). Closure of the gate has been proposed to occur by movement of the NT domain into the cytoplasmic vestibule of the hemichannel pore transduced through a straightening of a proline-kink in TM2 (Ri et al., 1999). The result is a local narrowing of the pore at the cytoplasmic vestibule that should also increase the effective charge density in this region. Oh et al. (1999) demonstrated in Cx32 that although open channel current is linear with V_j, the residual state rectifies such that current increases when the closed hemichannel is made relatively more negative. This observation is consistent with an increase in the electrostatic effect of a positive charge at the cytoplasmic vestibule of the hemichannel closed by fast V_j gate.

Previously, using Cx43 with EGFP fused to its CT domain, we determined that the hemichannel in response to applied V_j closes to the residual state on the relatively negative side. Accordingly, the sensor should be positively charged. Here, we examined whether the residual state exhibited rectification that is consistent with the introduction of a positive charge at the closed end of the Cx43 channel. Furthermore, we extended these studies to examine whether the Cx43 channel in the residual state indeed represents a narrowed pore and whether there is a change in the charge selectivity compared with the open state, as might be expected by the translocation of the NT domain. These were accomplished at the level of the single channel as well as macroscopically using protocols designed to close the fast, but not the slow, V_j gate (Bukauskas et al., 2001). Due to its stable conformation, as evidenced from its long dwell time, the residual state can play a significant functional role in regulating the transmission of electrical signals and the cell–cell transfer of metabolites.

MATERIALS AND METHODS

Cell Lines and Culture Conditions

Experiments were performed on HeLa cells (a human cervix carcinoma cell line; ATCC No. CCL-2) transfected with Cx43 or Cx43-EGFP and on Novikoff cells, a rat hepatoma cell line, that endogenously express Cx43 (Meyer et al., 1991). HeLa cells were stably transfected with cDNAs encoding rat Cx43 or rat Cx43-EGFP. The cDNA encoding Cx43-EGFP was constructed as described by Jordan et al. (1999). HeLa cells were grown in DME supplemented with 10% FBS. All media, sera, and culture reagents were obtained from Life Technologies (GIBCO BRL). The transfection procedure has been described previously (Jordan et al., 1999; Bukauskas et al., 2001). Novikoff cells were grown in Swim's S-77 medium with 4 mM glutamine, 20% horse serum, and 5% FBS. To study homotypic junctions, cells of one type were seeded at a density of $\sim 10^4$ cells/cm^2 onto sterile coverslips placed in culture dishes. To study Cx43/Cx43-EGFP heterotypic junctions, Novikoff cells were mixed with HeLaCx43-EGFP cells in equal quantities and seeded on coverslips at $\sim 10^4$ cells/cm^2. Novikoff cells were transferred to Dulbecco's medium 3 wk before coculturing with HeLa cells.

Electrophysiological Measurements

For simultaneous electrophysiological and fluorescence recording, cells were grown on 22 × 22-mm number 0 coverslips and transferred to an experimental chamber (Bukauskas, 2001) mounted on the stage of an inverted microscope (model Olympus IX70; Olympus America) equipped with phase-contrast optics and a fluorescence imaging system. The chamber was perfused with a modified Krebs-Ringer's solution containing the following (in mM): 140 NaCl, 4 KCl, 2 $CaCl_2$, 1 $MgCl_2$, 5 HEPES, 5 glucose, and 2 pyruvate, pH 7.4. In most of the experiments, patch pipettes were filled with our standard pipette solution containing the following (in mM): 10 NaCl, 130 KCl, 0.26 $CaCl_2$, 1 $MgCl_2$, 3 MgATP, 5 HEPES, pH 7.2, and 2 EGTA ($[Ca^{2+}]_i = 5 \times 10^{-8}$ M). Table I shows the compositions of the pipette solutions used in ion-substitution studies. Solutions were adjusted to pH 7.2 by using KOH for solutions 1 and 2, and TEAOH for solution 3. In addition, we measured conductivity of all pipette solutions using conductometer (Accumet model-30; Fisher Scientific).

g_j was measured using the dual whole-cell patch clamp (Neyton and Trautmann, 1985). Briefly, each cell of a pair was voltage-clamped independently with a separate patch clamp. By stepping the voltage in one cell and keeping the other constant, junctional current (I_j) is measured directly as a change in a current in the unstepped cell. Thus, g_j is obtained by dividing the change in

TABLE I

Composition of the Pipette Solutions Used in Ion Substitution Studies

Pipette solution	KCl	KAsp	TEACl	$CaCl_2$	EGTA	$MgCl_2$	HEPES	Conductivity
	mM	*mM*	*mM*	*mM*	*mM*	*mM*	*mM*	*mS/cm*
#1, KCl	140			0.26	2	1	5	17.2
#2, KAsp		140		0.26	2	1	5	12.1
#3, TEACl			140	0.26	2	1	5	11.3

I_2 by the change in V_1. With low levels of coupling, unitary junctional currents can be recorded as discrete quantal changes in the unstepped cell that are accompanied by equal and opposite quantal changes in the stepped cell. Voltages and currents were recorded on videotape using a data recorder (model VR-100; Instrutech), and digitized in parallel using a converter (model MIO-16X A/D; National Instruments) and our own acquisition software. Records were digitized at 5 kHz and filtered at 1 kHz. Junctional conductance is plotted in two ways: as the chord conductance (g_j) calculated as I_j/V_j and slope conductance (g_{jslope}) calculated as $\Delta I_j/\Delta V_j$, where $\Delta I_j = I_{j,n+1} - I_{j,n}$ and $\Delta V_j = V_{j,n+i} - V_{j,n}$; n is the nth point of a digitized current or voltage recording. To increase the signal to noise ratio, the values of ΔI_j and ΔV_j were calculated by using a running average procedure in which ~10–20 sequential digitized data points were averaged. We used g_{jslope} preferentially to study a rectification of macroscopic residual conductance by superposing repeated V_j ramps of small amplitude onto the V_j steps (see Fig. 1 C). g_{jslope} has some advantages over g_j because of the following: (1) slow variations of nonjunctional membrane as well as seal leak currents do not have an impact on calculated g_{jslope} value, whereas g_j depends on an absolute value of I_j; (2) g_{jslope} can be measured at V_js that are close to zero, whereas g_j deviates to infinity; and (3) g_{jslope} is better applicable to study conductance dependence on V_j for the processes with nonlinear I-V relationships.

Cx43-EGFP Fluorescence and Dye Transfer Measurements

Fluorescence signals were acquired and analyzed using an OlymPix 2000-cooled digital camera (12 bit) mounted on an Olympus IX70 microscope, a SpectraMASTER high speed monochromator, and UltraVIEW software for image acquisition and analysis (Perkin Elmer Life Sciences). The wavelengths used for excitation of EGFP, Alexa Fluor, and ethidium bromide were delivered by a monochromator and were 480, 350, and 518 nm, respectively. Appropriate filter cubes were used for monitoring emission (Chroma Technology Corp.).

For cell–cell dye transfer studies, three patch pipettes were used: two for dual whole-cell voltage-clamp recording, and a third for loading one cell of a pair with fluorescent dye. Dye was added to the third pipette at a concentration of ~0.1 mM. A dual whole-cell recording was established first, and a V_j was imposed before introducing the dye-filled pipette. This experimental design allowed us to load dye in one cell and monitor cell–cell transfer with GJ channels predominantly in the residual state. Offline analysis of fluorescence in both cells of a pair was accomplished using UltraVIEW software. Fluorescence intensity in each cell of a pair was measured as the average within a region of interest that included most of the area of the cell (see Fig. 7). Background fluorescence was measured in region of interest that is located outside the cell pair. All data are plotted as background-subtracted intensities.

RESULTS

Rectifying Properties of Macroscopic Residual Conductance of Cx43/C43-EGFP Channels

Recently, we showed that the fast gate, which closes channels to the residual state, and the slow gate, which closes channels completely, operate in series such that activation of the slow gate depends on whether the fast gate is open or closed (Bukauskas et al., 2001). At small V_js (up to ~60 mV), the fast gate remains open and most gating events reflect the operation of the slow gate. At V_js between ~60 and 100 mV, the faster and more steeply V_j-sensitive fast gate closes channels to the residual state, preventing closure of the slow gate due to a reduction in V_j across the slow gate. At sufficiently large V_js (i.e., >100 mV), the slow gate can close even with the fast gate closed. Thus, we used heterotypic Cx43/Cx43-EGFP junctions and the V_j "window" between ~60 and 100 mV at which most Cx43 channels reside in the residual state to examine and compare I-V characteristics of open and residual states. In this heterotypic pairing configuration, only the Cx43 hemichannels express fast V_j gating (i.e., close to the residual state; Bukauskas et al., 2001). Cx43/Cx43-EGFP cell pairs were obtained from cocultures of Novikoff cells, which endogenously express only Cx43, and HeLa cells transfected with Cx43-EGFP. Heterotypic cell pairs were identified by having only one cell of a pair displaying EGFP fluorescence (Fig. 1 A). The arrow in the example of the cell pair shown indicates a junctional plaque in the region of cell–cell contact. Fig. 1 B shows the asymmetric G_j-V_j dependence characteristic of Cx43/Cx43-EGFP junctions. Data are pooled from 19 cell pairs. Fast V_j gating of Cx43 hemichannels is manifest macroscopically as a reduction in g_j to a residual plateau value at large negative V_js on the Cx43 side. Conversely, g_j decreases to zero at large positive V_js, which is indicative of a lack of fast V_j gating to the residual state in Cx43-EGFP hemichannels (Bukauskas et al., 2000). The solid lines are fits of the data for each polarity of V_j to a Boltzmann relation of the form: $G_j = (1 - G_{min})/\{1 + \exp[A \cdot (V_j - V_0)]\} + G_{min}$, where G_{min} is the normalized residual g_j, A is a measure of voltage sensitivity in mV^{-1}, and V_0 is the V_j at which G_j is halfway between the maximum and minimum values. The Boltzmann parameters are as follows: $V_0 = 49 \pm 2$ mV, $A = 0.07 \pm 0.01$ mV^{-1}, and $G_{min} = 0.2 \pm 0.02$ for negative V_js and $V_0 = 66 \pm 2$ mV, $A = 0.07 \pm 0.02$ mV^{-1} and $G_{min} = 0.12 \pm 0.03$ for positive V_js. The dashed line shows the Boltzmann G_j-V_j relation obtained for homotypic Cx43 junctions (Bukauskas et al., 2001).

Examples of changes in I_j upon application of long duration V_j steps show that I_j declines rapidly to a residual steady-state level with negative V_j on the Cx43 (Novikoff) side. For the opposite polarity (i.e., positive on the Cx43 side), I_j declines considerably more slowly and fails to reach steady state within the 60-s duration of the V_j step (Fig. 1 C). These properties at negative and positive V_js relative to the Cx43 side are characteristic of gating ascribed to Cx43 and Cx43-EGFP hemichannels, respectively (Bukauskas et al., 2001). Correlative single-channel studies by Bukauskas et al. (2001) have shown that the rapid decline in g_j to the residual steady-state level reflects closure of Cx43 hemichannels to their residual state and the continued decline in g_j to near zero shows full closures of Cx43-EGFP hemichannels.

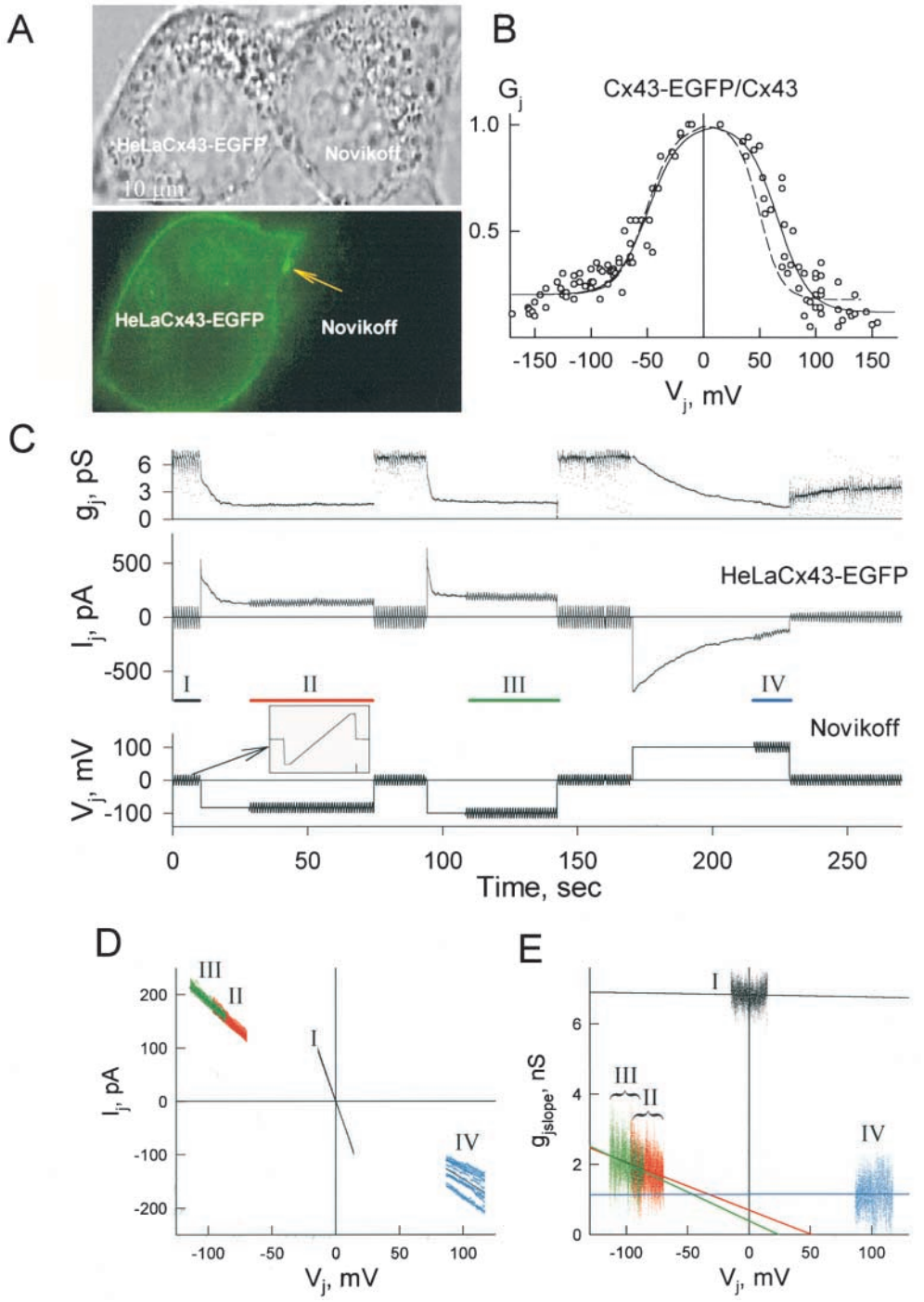

FIGURE 1. V_j gating of heterotypic Cx43/Cx43-EGFP junctions formed between Novikoff and HeLaCx43-EGFP cells. (A) Phase-contrast (top) and fluorescent (bottom) images of a Novikoff/HeLaCx43-EGFP cell pair. The fluorescent image shows diffuse distribution of Cx43-EGFP in the plasma membrane of the HeLaCx43-EGFP cell and punctate staining representing junctional plaques (arrow) in the region of contact with the Novikoff cell. (B) G_j-V_j dependence of Cx43/Cx43-EGFP heterotypic junctions with data pooled from 19 cell pairs. G_j represent g_j normalized to its value at $V_j = 0$ mV. For each data point, g_j was measured at the end of a 30-s V_j step. Positive and negative V_js correspond to the Novikoff cell made relatively positive and negative, respectively. The solid lines for each polarity of V_j are fits of the data to the Boltzmann relation. The dashed line shows the Boltzmann G_j-V_j relation of homotypic Cx43 junctions (Bukauskas et al., 2001). (C) Selected examples illustrate differences in the kinetics of V_j dependence at positive and negative V_j steps applied to the Novikoff cell. Repeated ±14-mV pulses (inset) were applied between and on the top of V_j steps of −80, −100, and +100 mV to monitor junctional conductance. (D) I-V scatter plots obtained from the intervals I–IV indicated in C. The I-V plot obtained from time interval I corresponds to the open state and is linear. The I-V plots obtained from intervals II (red line) and III (green line) correspond to the residual state of the Cx43 hemichannel and show a small degree of rectification. The I-V (blue) plot obtained from interval IV (blue line) also corresponds to the open state, but shows variability among individual ramps as a result of continued decline in conductance with slow gating. (E) Corresponding g_{jslope}-V_j scatter plots from the intervals I–IV shown in C. Solid lines are linear regressions illustrating the lack of V_j dependence for channels in the open state and modest V_j dependence for channels in the residual state.

To examine the I-V characteristics of junctions in open and residual states, repeated small amplitude V_j ramps (Fig. 1 C, inset) were applied at times in between and superimposed onto the V_j steps (Fig. 1 C). Corresponding I_j-V_j and g_{jslope}-V_j scatter plots were obtained from ramps applied during the indicated intervals, I–IV, (Fig. 1, D and E; for g_{jslope} calculations see MATERIALS AND METHODS). The I-V relations obtained from ramps applied with cells held at $V_j = 0$ (interval I) were stable and linear, giving a g_{jslope} of ~6.8 nS. The I-V re-

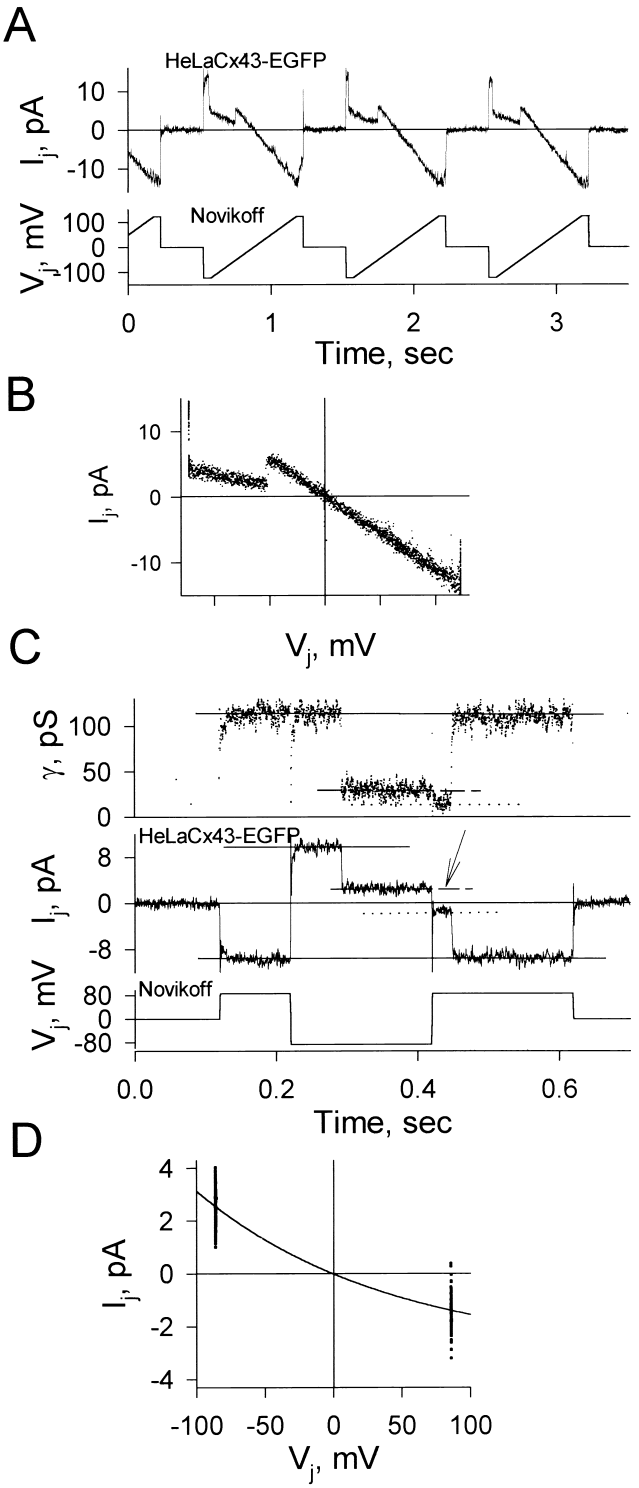

FIGURE 2. I_j-V_j relationship of a single-channel recorded in Novikoff/HeLaCx43-EGFP cell pair. (A) The voltage protocol applied to the Novikoff cell consisted of repeated (1 s) ramps from −120 to +120 mV initiated and terminated by 50-ms epochs at −120 and +120 mV. The I_j record shows gating transitions between open and residual states only at negative V_j. The channel typically reopens when V_j approaches 0 mV and stays open at positive V_j. (B) I_j-V_j scatter plot of all data points from A. (C) Representative example of a V_j polarity reversal protocol used to examine the residual state current at positive V_js. Stepping to +85 mV shows the open channel current giving γ_{open} = 115 pS; no gating to the residual substate is observed. Reversal to V_j = −85 mV results in equal, but opposite, current giving the same γ_{open} before eventually gating to the residual state (γ_{res} = 28 pS, dashed line). Upon reversal back to V_j = +85 mV, the channel briefly remains in the residual state before opening, and shows a reduced γ_{res} of 15 pS (dotted line). (D) I-V_j scatter plot obtained from the record presented in C. The solid line is a fit of the data by using single exponential function, $I_{jres} = I_o \cdot (\exp(b \cdot V_j) - 1)$. The fitting parameters were as follows: I_o = 3.3 ± 0.4 pA, b = −0.007 ± 0.001 mV^{-1} (n = 2,489); γ_{res} of Cx43/Cx43-EGFP channel rectifies decreasing nearly twofold when V_j changes from −100 to 100 mV.

lations obtained from V_j ramps superimposed onto the long duration V_j steps of −80 and −100 mV relative to the Cx43 side (intervals II and III, red and green, respectively) were also stable, but reduced in slope due to gating to the residual state and give g_{jslope}-V_j relations that show dependence on V_j (Fig. 1 E). The mean values of all data points calculated separately for g_{jslope} measured at V_j steps of −80 and −100 mV were 1.86 ± 0.01 nS (n = 18,426), and 2.03 ± 0.01 nS (27,384), respectively. The I-V relations obtained from V_j ramps superimposed onto the long duration V_j step of +100 mV relative to the Cx43 side (interval IV, blue) showed a reduced slope and, in addition, high variability among the individual ramps due to the fact that I_j was not at steady state and continued to decline. However, the I-V relations are linear, giving constant g_{jslope}-V_j relations much like that at V_j = 0. The mean value for g_{jslope} in this interval was 1.20 ± 0.01 nS (n = 7,762). Similar results of I-V characteristics were observed in nine other cell pairs. Given that these channels are predominantly open near V_j = 0 and gate only between open and closed states at V_js relatively positive on the Cx43 side, the linear I-V characteristics obtained at intervals I and IV are the result of current flow through open channels. Conversely, at V_js relatively negative on the Cx43 side (intervals II and III), channels are predominantly in the residual. These data are consistent with linear and rectifying properties of single channels in open and residual states, respectively.

I-V Characteristics of the Residual State of Cx43 at the Single-Channel Level

I-V curves at a single-channel level were examined in poorly coupled Novikoff/HeLaCx43EGFP cell pairs. In the example shown in Fig. 2 A, a V_j protocol consisting of repeated 600-ms ramps from −120 to +120 mV initiated and terminated by brief, 50-ms epochs at −120 and +120 mV, respectively, were applied to the Novikoff (Cx43) cell of a Novikoff/HeLaCx43EGFP cell pair containing a single functional channel. Gating transitions between open and residual states were observed only in the negative limb of the ramp. If the channel closed to the residual state at large negative V_js, then it typically re-

mained in the residual state until V_j decreased to about −50 mV whereupon it reopened and remained open throughout the remainder of the ramp. A plot of all the I_j data points versus V_j obtained from the three consecutive ramps in Fig. 2 A illustrates this behavior (Fig. 2 B) and is consistent with fast V_j gating being operational only in Cx43 hemichannels at relatively negative V_js on the Cx43 side. The lack of full closures characteristic of slow V_j gating at either V_j polarity is due to the slow kinetics of this gating mechanism; closures would be rare within the duration of ramps imposed.

Because the fast V_j gate in Cx43 hemichannels invariably reopens when the voltage ramps approach 0 mV, it was not possible using a ramp protocol to observe the I-V relation of the residual state at positive V_js. Alternatively, we applied a pulse protocol in which a single channel was driven into the residual state by applying a large conditioning V_j step negative to the Cx43 side and then reversing the V_j polarity. Typically, a channel remained in the residual state sufficiently long after polarity reversal to measure conductance at V_js positive on the Cx43 side (Fig. 2 C). An example is shown for an −85-mV conditioning step followed by reversal to +85 mV applied to the Novikoff (Cx43) cell of a Novikoff/Cx43-EGFP cell pair. Junctional conductance is plotted above the I_j record. For both positive and negative 85-mV V_j steps, open channel conductance (γ_{open}) was found to be the same (∼115 pS), which is consistent with V_j independence of the open state conductance, whereas the residual conductance (γ_{res}) was ∼28 pS for −85 mV (Fig. 2 C, dashed line) and ∼15 pS for +85 mV (Fig. 2 C, dotted line), which is consistent with the rectification previously indicted in macroscopic experiments. Fig. 2 D shows a γ_{res}-V_j scatter plot of the data presented in Fig. 2 C. The solid line is an exponential fit to the data constrained to go through the origin.

Fig. 3 (A and B) combines scatter plots of all data points that were collected by using voltage ramp and step protocols for open and residual states, respectively. The I_j-V_j scatter plot for the open state is well fit by a linear relation (Fig. 3 A, solid line) giving γ_{open} = ∼115 pS (35 ramps from four experiments). The I_j-V_j plot for the residual state shown in Fig. 3 B was collected from 25 records using voltage ramp protocol (four experiments) and 12 records (three experiments) using voltage step protocol. The I_j-V_j data are fit well by an exponential function with γ_{res} decreasing from ∼28 pS at V_j = −100 mV to ∼15 pS at V_j = 100 mV. Correspondingly, the ratio, $\gamma_{res}/\gamma_{open}$, decreases from 0.23 to 0.13 (Fig. 3 C).

We sought to confirm our findings in homotypic Cx43 channels because of the possibility that the residual state of Cx43 hemichannels has different characteristics when paired heterotypically with Cx43-EGFP hemichannels. Such measurements were accomplished by V_j polarity reversal experiments designed to capture

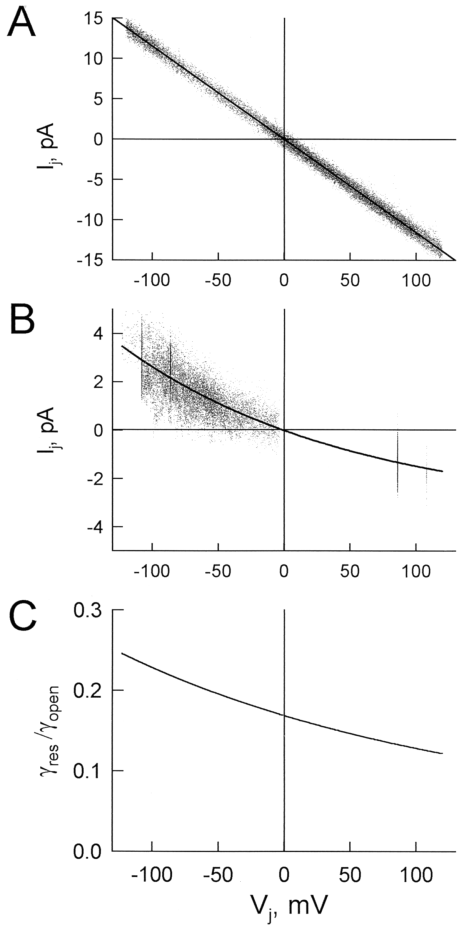

FIGURE 3. Summarized I_j-V_j plots for open and residual states obtained from voltage ramp and step protocols. (A) I_j-V_j scatter plot of the open state (35 ramps from four different cell pairs). The slope of a linear regression (solid line) gives γ_{open}= 115 pS (r^2 = 0.99; n = 9,200 data points). (B) I_j-V_j scatter plot for the residual state obtained from 25 records using the voltage ramp protocol and 12 records using the voltage step protocol. The solid line is an exponential fit of the data. Fitting parameters are as follows: I_o= 3.5 ± 0.2 pA, b = −0.0053 ± 0.0002 mV^{-1} (n = 18,500 data points). (C) A $\gamma_{res}/\gamma_{open}$-$V_j$ plot shows that the ratio $\gamma_{res}/\gamma_{open}$ decreases nearly twofold over a ±100-mV V_j range.

the residual state of one hemichannel over a wide range of V_j. Fig. 4 A shows an example of a single-channel current record in which a V_j of −70 mV was applied by hyperpolarizing cell 1 to place the hemichannel in this cell into the residual state (Fig. 4 A, dashed line). Holding potentials of −75 and −5 mV were applied to cell 1 and cell 2, respectively. Intermittent, short duration (100 ms) steps to a positive V_j were applied to measure I_j of the residual state upon polarity reversal. The insert shows an expanded view of one of the V_j reversals. The residual state displays a conductance of ∼30 pS at V_j = −70 mV (Fig. 4 A, dashed line) and decreases to ∼18 pS at +35 mV. Fig. 4 B shows an I-V scatter plot of data obtained from four cell pairs (two Novikoff cell pairs and two Cx43-transfected HeLa cell

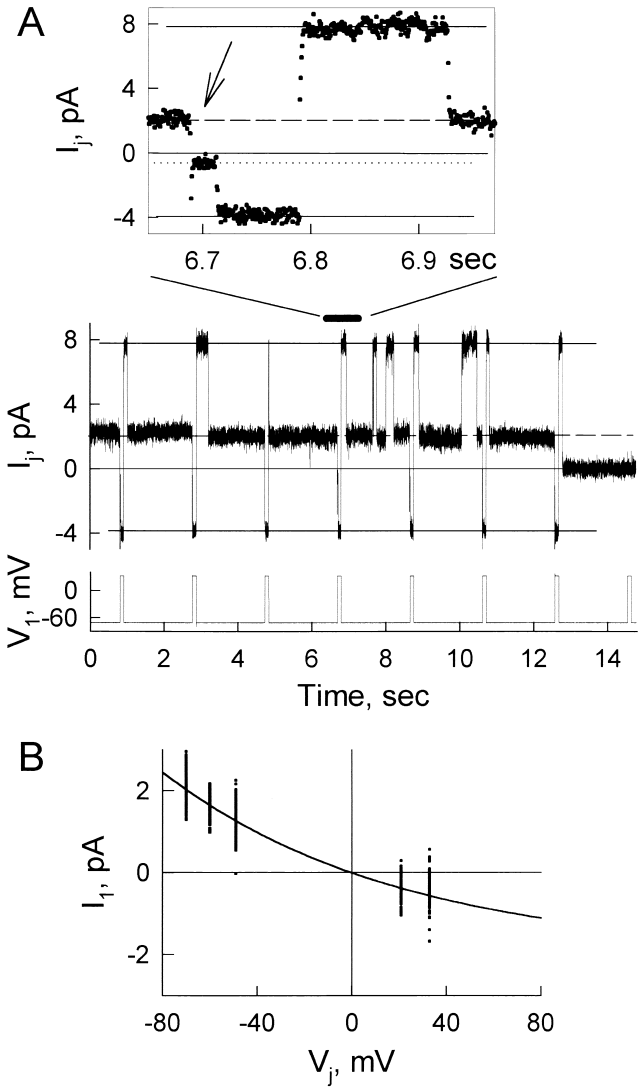

FIGURE 4. Residual conductance dependence on V_j in Cx43 homotypic channels. (A) I_j record obtained in the late stage of CO_2-induced uncoupling in a HelaCx43 cell pair when only a single channel was operating. The holding potential in cell 1 was −75 mV, and in cell 2 was −5 mV; repeated pulses of +105 mV were applied to cell 1. V_j of −70 mV was maintained throughout except for intermittent pulses. The channel predominantly resides in the residual state at $V_j = -70$ (dashed line). Upon V_j reversal to +35 mV, the channel briefly remains in γ_{res} before opening fully (lower solid line). At the end of this record, the channel closed fully (i.e., to a nonconducting state), as evidenced by a lack of a change in I_j in response to the last V_j step. Inset shows I_j during V_j reversal at an extended time scale. I_j at $V_j = +35$ mV gave a residual conductance of ~18 pS (dotted line) compared with γ_{res} of ~30 pS at $V_j = -70$ mV (dashed line). (B) I_j-V_j scatter plot of the residual state obtained from the data shown in A and three other similar experiments. The solid line shows the fit of the data to a single exponential function. The fitting parameters were as follows: $I_o = 1.5 \pm 0.5$ pA, and $b = -0.011 \pm 0.003$ mV^{-1} ($n = 894$ data points).

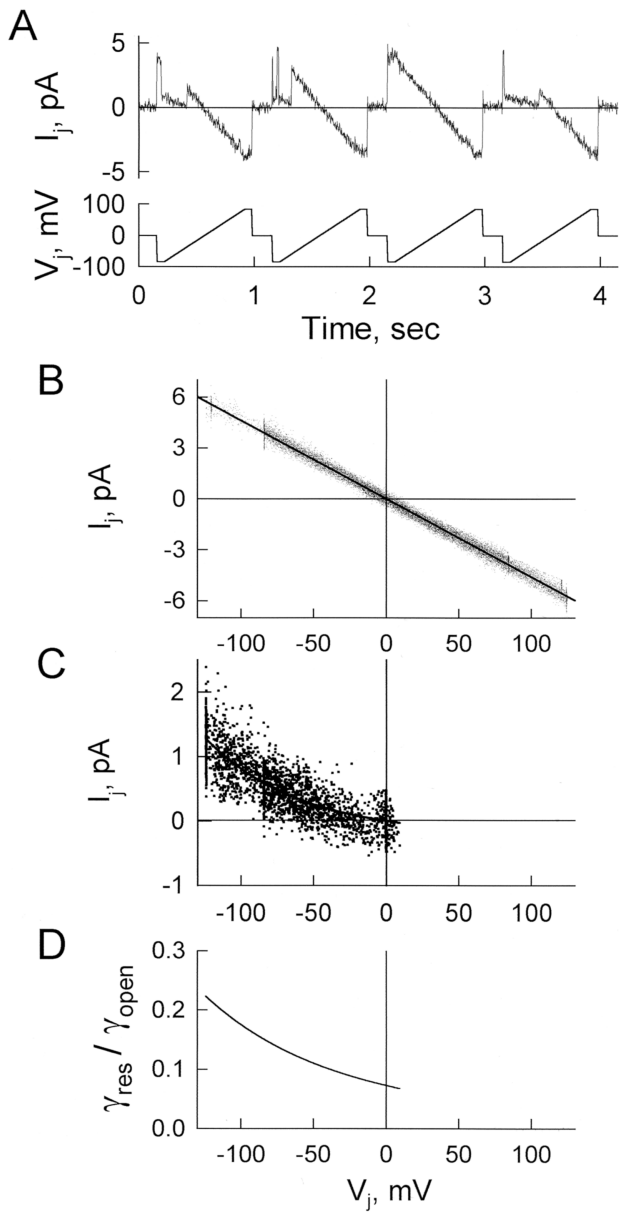

FIGURE 5. Rectification of the residual state in symmetric KAsp. (A) Single-channel currents in a Novikoff cell pair in response to repeated V_js ramps (from −85 to 85 mV) demonstrates gating transitions between open and residual states. (B) Summarized I_j-V_j scatter plot of data points from the open state. A linear regression (solid line) gives an open channel conductance of 46 pS (n = 9,100 data points; $r^2 = 0.99$). (C) Summarized I_j-V_j scatter plot of data points from the residual state (collected from five cell pairs). A fit to a single exponential function gave parameters as follows: $I_o = 0.22 \pm 0.03$ pA, and $b = 0.016 \pm 0.002$ mV^{-1} ($n = 2{,}920$ data points; solid line). (E) $\gamma_{res}/\gamma_{open}$-$V_j$ scatter plot calculated from the fitted curves shown in B and C. $\gamma_{res}/\gamma_{open}$ declines from ~0.18 to ~0.07 when V_j changes from −100 to +6 mV.

pairs), and is indistinguishable from that obtained in heterotypic Cx43/Cx43EGFP channels, with the Cx43 side made relatively negative. Unlike the heterotypic channel, the same degree of rectification, but opposite in direction, could be obtained in the homotypic channel for either polarity of V_j. These results indicate that the conductance and I-V characteristics of the residual

state of a Cx43 hemichannel are the same whether incorporated in a homotypic Cx43 channel or heterotypic Cx43/Cx43-EGFP channel.

The Open and Residual States Differ in Selectivity

To assess selectivity of the residual state, we examined changes in conductance of open (γ_{open}) and residual (γ_{res}) states upon ion substitution. Compositions of the pipette solutions used in these experiments are shown in Table I. Removal of MgATP and NaAsp from the standard KCl solution (solution #1), had no appreciable affect on conductance of either the open or residual states, as well as on sensitivity of V_j gating of homotypic Cx43 channels. Upon replacement of Cl^- with Asp^-, the I-V relation of the open channel, obtained from repeated voltage ramps, remained linear, but conductance decreased from 115 pS to ~45 pS, which is suggestive of a substantial anionic component to the current flowing through the open state (Fig. 5 A). Data showing I_j-V_j plots of open and residual state obtained from five experiments are shown in Fig. 5 (B and C, respectively). The slope of the regression line from (Fig. 5 B, solid line) yields a conductance of 46 pS (n = 9,100 data points; $r^2 = 0.99$) for the open state. Conductance of the residual state decreased from ~10 pS at $V_j = -120$ mV to ~3 pS at $V_j = 0$ mV; at positive V_js, current in the residual state was too small to measure reliably (Fig. 5 C). A plot of the ratio, $\gamma_{res}/\gamma_{open}$, illustrates the steeper rectification in KAsp compared with KCl and is consistent with an increase in anion selectivity of the residual state (Fig. 5 D).

We performed the same set of experiments upon replacement of K^+ with TEA^+ (Fig. 6). Like in KAsp, conductance of the open channel in TEACl also decreased substantially, from ~115 to ~40 pS, and the open state I-V curve remained linear (Fig. 6 B). These data suggest that K^+ contributes to the conductance of the open state comparably to Cl^-. The conductance of the residual state also decreased, but the I-V relation in TEACl showed substantially weakened rectification, giving a nearly constant value for $\gamma_{res}/\gamma_{open}$ between −100 and +100 mV (Fig. 6 D). Thus, at positive V_js relative to the side of a closed hemichannel, γ_{res} is reduced substantially more upon replacement of Cl^- than K^+, which again is consistent with an increased anion selectivity of the residual state.

Confirmation of the selectivity properties of the residual state using measurement of reversal potential was not successful because large V_js were needed to keep channels in the residual state and they tended to open in the V_j range where current reversal would occur. At the single-channel level, reversal potential was difficult to assess with confidence as the substate currents in the substituted salts were small and often within the noise of the whole-cell recording.

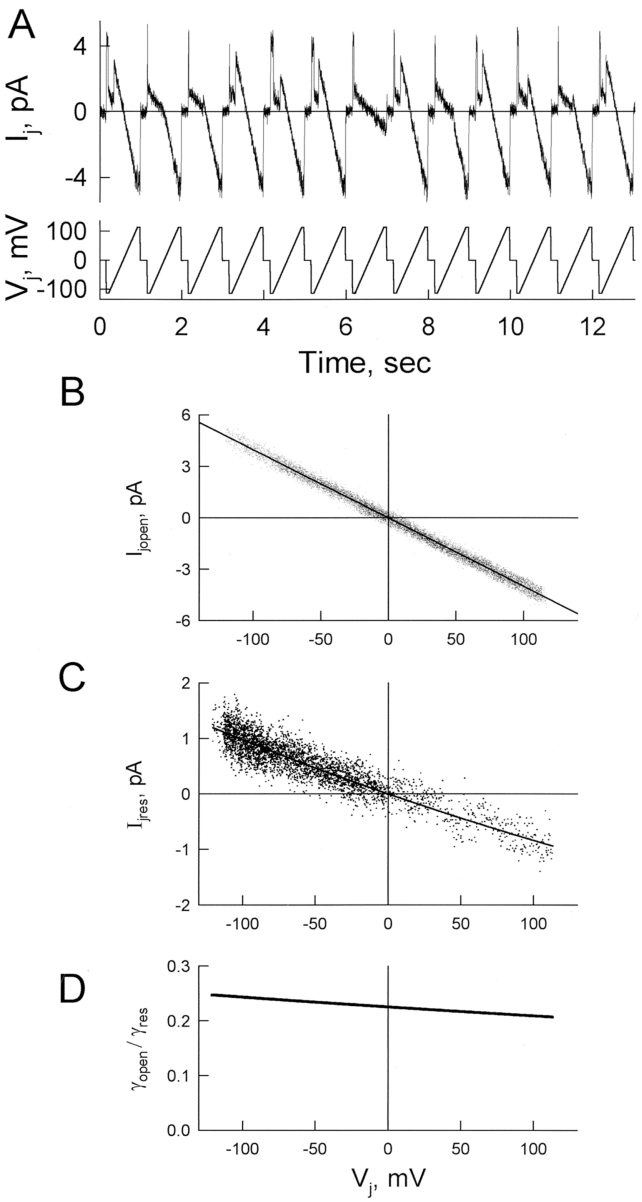

FIGURE 6. Rectification of the residual state in symmetric TEACl. (A) Single-channel currents in a Novikoff cell pair in response to repeated V_j ramps (from −85 to 85 mV) demonstrate gating transitions between open and residual states. (B) I_j-V_j scatter plot of data points corresponding to the open state collected from four cell pairs. The slope of the regression line (solid line) gives a conductance of 40 pS (n = 10,328 data points; $r^2 = 0.99$). (C) I_j-V_j scatter plot for the residual state collected from four cell pairs shows little rectification. The fitting parameters to a single exponential function were as follows: $I_o = 0.22 \pm 0.03$ pA, and $b = -0.016 \pm 0.002$ mV^{-1} (n = 3,584 data points; solid line). (D) $\gamma_{res}/\gamma_{open}$-$V_j$ scatter plot calculated from the fitted curves shown in B and C. $\gamma_{res}/\gamma_{open}$ declines from ~0.25 to ~0.21 when V_j changes from −100 to +100 mV.

Permeability of the Residual State of Cx43 Channels to Dyes

A different assessment of perm-selectivity also can be obtained from dye flux studies. To examine dye permeability of the residual state, we needed to impose a large V_j between Novikoff cells during dye transfer and

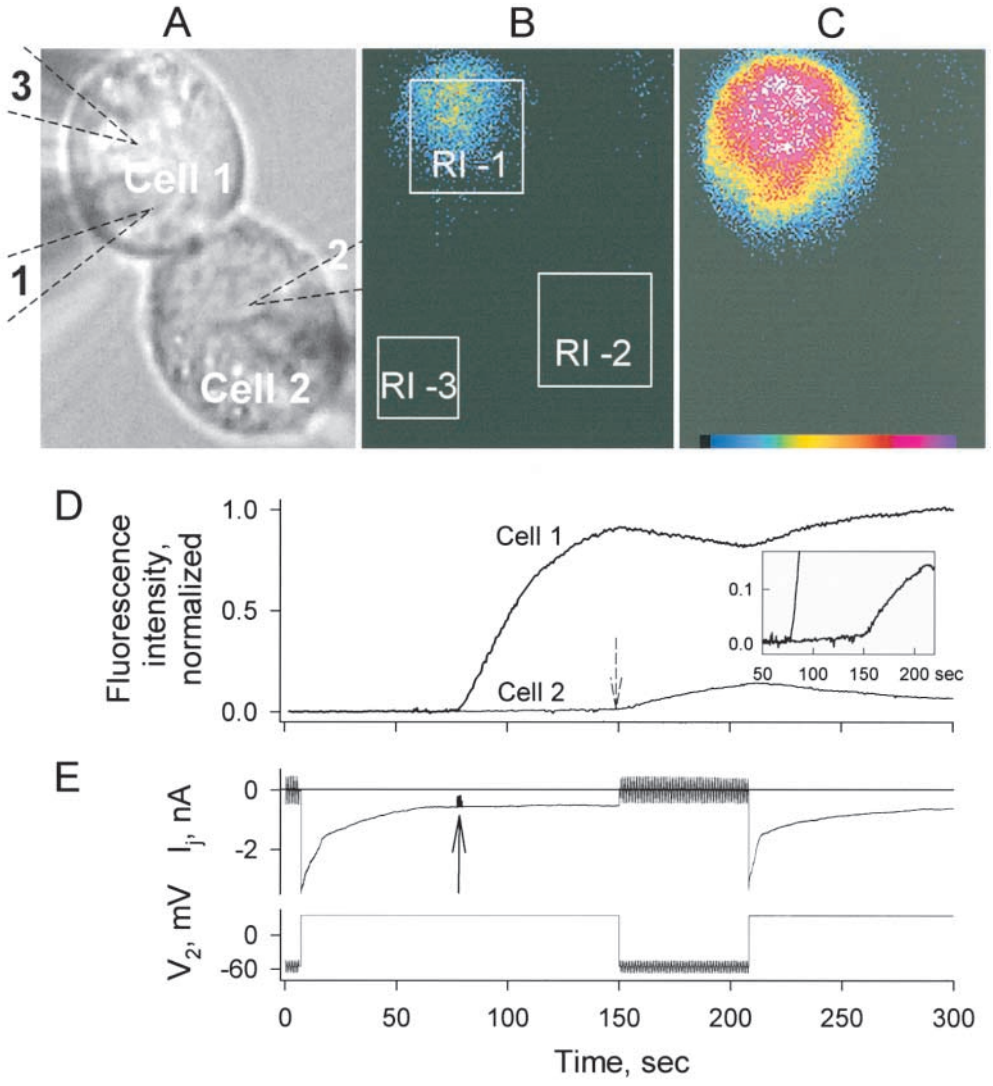

FIGURE 7. Intercellular transfer of Alexa Fluor, a negatively charged dye, is restricted when channels are in the residual state. (A–C) Phase-contrast (A) and fluorescence (B and C) images showing a Novikoff cell pair in which dye transfer and coupling were examined in open and residual states. Locations of pipettes 1 and 2 used for dual voltage clamp recording and pipette 3 used for loading cell 1 with dye are indicated. RI-1, RI-2, and RI-3 are regions of interest from which fluorescence intensities were measured. Fluorescence intensities in the cells were calculated by subtracting the background fluorescence (RI-3) from the fluorescence measured in RI-1 and RI-2. (D) Plot of fluorescence intensity normalized to the maximum (NFI) in cell 1 and cell 2 over time. NFI in cell 1 rises upon opening the patch in pipette 3 (arrow) and reaches a plateau after ~70 s. NFI in cell 2 shows little change during the time V_j is imposed when channels mainly reside in the residual state. Upon reopening channels by removal of V_j, NFI begins to rise immediately and reaches ~14% of the maximum within 60 s (inset shows an expanded scale of NFI). Concomitant with an increase in NFI in cell 2, there is a decrease in cell 1, presumably due to rapid dye transfer to cell 2. Reimposition of V_j caused an immediate decline in NFI in cell 2 due to loss of transfer from cell 1 and dialysis with patch pipette 2. (E) Records of I_j and V_2 over time corresponding to fluorescence plot in D. V_j of +90 mV was applied to cell 2 which caused g_j to decline to a steady-state value of ~10 nS. Between 90-mV V_j steps, small repeated ±10-mV V_j steps were applied to cell 2 to assess g_j, which remained constant at 43 nS. Conductance recovered rapidly upon removal of the +90-mV V_j step. Arrow indicates opening of the patch in pipette 3.

modified the protocol to include the use of three patch pipettes: two for dual whole-cell voltage-clamp recording, and a third pipette to load one of the cells with dye. Fig. 7 A shows a phase-contrast image of a cell pair with positions of the three pipettes outlined (Fig. 7 A, dashed lines). After gigaohm seals were formed with all three pipettes, whole-cell recordings were established with pipettes 1 and 2. Both pipettes were held at a common voltage of −55 mV to maintain $V_j = 0$ mV. A g_j of 43 nS, corresponding to ~390 open channels on average, was measured by applying repeated small, brief V_j steps to cell 2. A large, long duration 90-mV V_j step was then applied by depolarizing cell 2 to close channels to their residual state (Fig. 7 E). This V_j step would tend to close the Cx43 hemichannels in cell 1 to their residual state. Upon reaching a steady-state current, a whole-cell recording in current clamp mode was established in cell 1 with the third patch electrode filled with Alexa Fluor to initiate dye loading (Fig. 7 E, arrow). Fluorescence images taken 2 and 15 s after the start of dye loading are shown in Fig. 7 (B and C). The time course of fluorescence changes in both cells is plotted in Fig. 7 D. Fluorescence intensity rapidly rose in cell 1 after opening the dye-filled patch pipette, but almost no fluorescence was detected in cell 2. Note that V_j was such that cell 2 was relatively positive, which would assist transfer of the negatively charged Alexa Fluor. The slight amount of dye transfer detected was much less

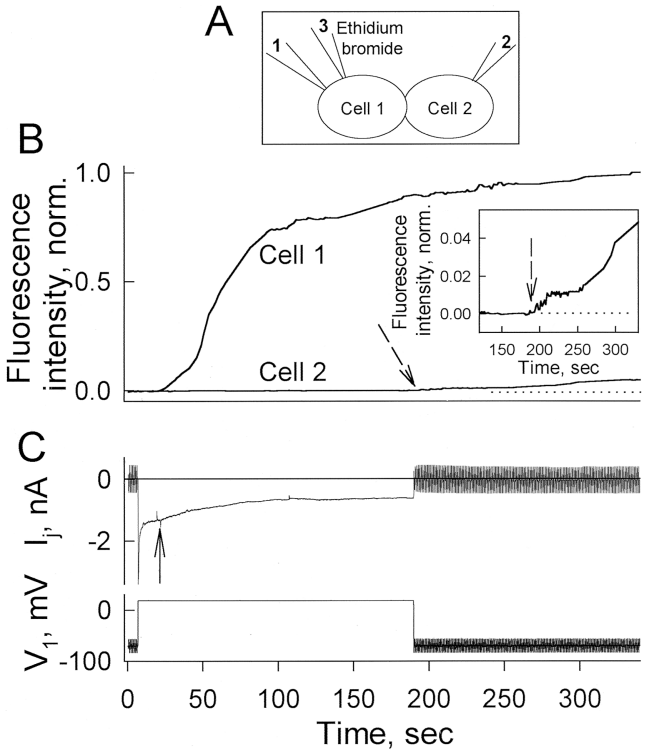

FIGURE 8. Intercellular transfer of ethidium bromide, a positively charged dye, is restricted when channels are in the residual state. (A) Schematic of a cell pair and the arrangement of pipettes used for recording and dye-loading. Fluorescence was measured in Novikoff cell pairs as described in Fig. 7. (B) Plot of NFI in cell 1 and cell 2 over time. NFI in the cell 1 increases upon opening the patch in pipette 3 (solid arrow) and approaches a plateau in ~100 s. NFI in cell 2 shows no change during the time a V_j step of +90 mV was imposed and channels mainly reside in the residual state. Upon reopening channels by removal of V_j, NFI begins to rise and reaches ~5% of the maximum within 150 s (inset shows an expanded scale of NFI; horizontal dotted line indicates zero fluorescence level). (C) Records of I_j and V_2 over time corresponding to fluorescence plot in B. V_j of +90 mV was applied to cell 2, which caused g_j to decline to a steady-state value of ~9 nS. Small repeated ±12-mV V_j steps were used to assess g_j, which recovered rapidly up to 35 nS level upon a removal of long +90 mV V_j step.

than that expected by the decrease in conductance, and can be explained by a small number of channels opening occasionally (Fig. 7 D, inset). Upon removal of V_j, conductance rapidly recovered and fluorescence immediately started to rise in cell 2 concomitant with a decrease in fluorescence in cell 1. These results are indicative of rapid flux of dye from cell 1 into cell 2. A second depolarization of cell 2 by 90 mV again halted dye flux into cell 2; the decrease in fluorescence in cell 2 is likely due to dye loss into the patch pipette. Four additional experiments similarly showed no appreciable transfer of Alexa Fluor through Cx43 GJ channels residing in the residual state.

A similar result was obtained using ethidium bromide, except that the rate of fluorescence rise in cell 1 and cell 2 was less than that of Alexa Fluor (Fig. 8). The cell pair in the example shown had a g_j= 35 nS. No transfer of ethidium bromide was detectable while the channels were in the residual state. Dye transfer immediately followed removal of the imposed V_j (Fig. 8 B, inset). As previously shown, recovery from closure to the residual state in Cx43 channels is rapid, within a few seconds (Bukauskas et al., 2001). In this experiment, V_j was such that cell 1 was relatively positive, which would assist transfer of the positively charged ethidium bromide. Similar results were obtained in four other cells pairs with conductance ranging from 20 to 55 nS.

DISCUSSION

In this paper, we sought to examine the conductance and permeability properties of the residual state of Cx43 GJ channels. The finding that GJ channels are sensitive to V_j demonstrated the distinctive property of residual conductance in which g_j declines to a nonzero conductance plateau (Harris et al., 1981). The residual g_j resembles a voltage-insensitive conductance whose magnitude has been shown to be connexin-specific, ranging from a small fraction to as large as ~30% of the maximum g_j (Werner et al., 1989; Willecke et al., 1991; Rook et al., 1992; Moreno et al., 1995; White et al., 1995; Steiner and Ebihara, 1996; Revilla et al., 1999). Single-channel studies have shown that the residual g_j is explained by gating of GJ channels to a long-lived substate (Weingart and Bukauskas, 1993; Moreno et al., 1994). Weingart and Bukauskas (1993) termed this substate as the "residual state" and demonstrated it to be a property of different connexins (Bukauskas et al., 1995; Bukauskas and Peracchia, 1997; Valiunas et al., 1997), and proposed that the residual state represents the maximally closed state for this gate. GJ channels also can close completely (i.e., to a nonconducting state in response to V_j or V_m; Bukauskas and Weingart, 1994; Banach and Weingart, 2000), but we have shown that full closures are the result of a separate gate (Bukauskas et al., 2000, 2001).

Although in most homotypic channels large V_js are often necessary to invoke gating to the residual state, heterotypic channels can have g_j-V_j relations that are shifted so strongly that most of the time the channels reside in the residual state at V_js close to zero. Our unpublished data as well as data of Elenes et al. (2001) show that a substantial fraction of heterotypic Cx45/Cx43 or Cx45/Cx47 channels are closed at V_j = 0 mV by reason of high V_j sensitivity of the slow gating mechanism. In addition, V_j gating sensitivity of Cx45/Cx43 or Cx45/Cx47 channels at V_js relatively negative on Cx45 hemichannel side is almost twice higher than V_j gating sensitivity of homotypic Cx45 channels. This effect may be due to the relatively small unitary conductance of Cx45 hemichannel in comparison with unitary conductance of Cx43 or Cx47 hemichannel. Thus, het-

erotypic channels can be largely gated to closed or to the residual states at V_js close to zero.

Studies of the residual state must keep in mind that GJ channels are composed of two hemichannels that can be the same or different. V_j gating, being a property intrinsic to the hemichannel (Trexler et al., 1996; Oh et al., 2000), means that GJ channels possess two sets of gates that are oppositely oriented with respect to the field generated by V_j. Thus, imposition of a V_j of a given polarity tends to close one hemichannel and keep the other open or even promote its opening if it was closed. The opposite polarity of V_j reverses this configuration. I-V curves for the residual state derived from I_j transitions induced by positive and negative voltages applied to one cell of a pair are not likely the result of closure of the same hemichannel and, thus, do not provide a measure of the I-V characteristics of the residual state. Using a combination of V_j ramp and step protocols, we were able to show at macroscopic (Fig. 1) and single-channel (Figs. 2–4) levels that the residual state of Cx43, when generated by V_j gating of one of the hemichannels, displays I_j rectification. In symmetric KCl solutions, the I_j rectification is larger when the gated hemichannel side is relatively negative. Gating by V_j in Cx43 homotypic channels is such that the hemichannel on the relatively negative side closes to the residual state. In Cx43 homotypic channels, rectification of the residual state is moderate, changing approximately twofold over a range of ±100 mV.

Oh et al. (2000) similarly demonstrated I_j rectification of the residual state in homotypic Cx32 GJ channels. Like in Cx43 GJ channels, gating by V_j in Cx32 is such that the hemichannel on the relatively negative side of the channel closes to the residual state. Interestingly, the direction of rectification is the same as in Cx43, with larger current flowing through the residual state when the closed hemichannel side is made relatively negative. These data are consistent with a mechanism proposed for V_j gating to the residual state that involves the formation of a gating barrier by charges in the NH_2 terminus. Mutational studies have shown that the V_j sensor is composed of a charge complex located in the NH_2 terminus whose net charge can be of either sign, and whose movement toward the channel pore is associated with hemichannel closure to the residual state (Verselis et al., 1994; Oh et al., 2000). Hemichannels that close at relative negativity on their side, such as Cx32 and Cx43, should contain a positively charged NH_2-terminal sensor. This form of voltage dependence is only sensitive to V_j and is insensitive to the cells' plasma membrane voltage (Verselis et al., 1991). For this reason, the voltage sensor has been proposed to be positioned in the pore where the transjunctional field would be constant for the same V_j regardless of the cells' transmembrane voltage (Harris et al., 1981). From modeling studies with Poisson-Nernst-Plank (PNP) theory (Chen and Eisenberg, 1993), Oh et al. (1999) proposed that the conformational change associated with V_j gating involves a narrowing of the cytoplasmic entry of the channel that increases the electrostatic influence of the NH_2-terminal sensor on ionic flux through the pore. This electrostatic influence creates an asymmetric charge profile within the pore that produces I_j rectification. For both Cx32 and Cx43, the gating barrier should be positively charged and would tend to produce the same direction of rectification in both types of channel. Our data are consistent with this mechanism for V_j gating.

According to this mechanism for V_j gating, closure of one hemichannel to the residual state should not only produce channel rectification, but also should change the charge selectivity characteristics of the channel. In addition, the concomitant narrowing of the pore should reduce the cutoff size for permeant molecules. Neither of these possibilities had been tested previously, and we used a combination of ion substitution and dye flux approaches. Replacement of either K^+ with TEA^+or Cl^- with Asp^- results in a substantial reduction in the open state conductance. This result can be explained if both K^+ and Cl^- contribute substantially to the current flowing through the open channel and is consistent with our previous studies using measurements of E_{rev} in KCl gradients that showed no appreciable selectivity between monovalent inorganic ions on the basis of charge (Trexler et al., 2000). However, the same substitutions had substantially different effects on the residual state. Fig. 9 A summarizes the data for three different pipette solutions, plotted as the ratio of residual to open channel conductance, $\gamma_{res}/\gamma_{open}$ as a function of V_j. Over most of the V_j range between ±125 mV, $\gamma_{res}/\gamma_{open}$ is substantially smaller in KAsp than in KCl and rectification is considerably steeper. Conversely, this ratio is larger in TEACl and rectification is nearly absent. A γ-ρ plot shown in Fig. 9 B demonstrates the dependence of single-channel conductance on the conductivity of the pipette solutions. Closed circles correspond to the conductance of the open state, and open circles to γ_{res} evaluated at $V_j = 0$ mV. Closed and open triangles show γ_{open} and γ_{res}, respectively, when pipette solutions contained mainly TEA^+Asp^- (Valiunas et al., 1997). Solid and dashed lines are regression curves of the second order calculated for open and residual states, respectively; dotted lines show confidential intervals separately for each regression line.

To qualitatively evaluate our results, we used 1-D PNP model (Chen and Eisenberg, 1993) to test whether a charge profile that introduces positive charge at one end of the channel can qualitatively explain the data. Fig. 10 A shows a schematic of the channel pore as a cylinder 100 Å in length and 10 Å in diameter. A charge locus is shown as a square, and z indicates the number of elementary charges. Fig. 10 B shows a family of I_j -V_j

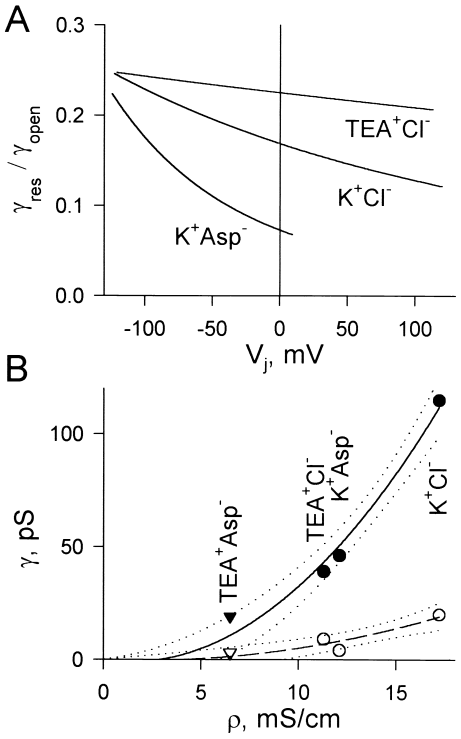

FIGURE 9. (A) Summarized $\gamma_{res}/\gamma_{open}$-$V_j$ plots (from experimental data) for three different pipette solutions. Rectification is steeper in symmetric KAsp and reduced in symmetric TEACl. (B) Plot of single-channel conductance versus conductivity of the pipette solutions. Closed and open circles correspond to γ_{open} and γ_{res}, respectively. Closed and open triangles are data for γ_{open} and γ_{res}, respectively, in symmetric TEA^+Asp^- taken from Valiunas et al. (1997). Solid and dashed lines are regression lines of the second order for γ_{open} and γ_{res}, respectively; dotted lines show confidential interval.

curves for the channel bathed in symmetric 140 mM KCl with z = +6 or z = −6 and located at different locations along the pore (symbol on the curve corresponds to the symbol shown in Fig. 10 A). These I_j-V_j plots show that a positive charge induces rectification of the I-V plot, resulting in a conductance decrease when V_j changes from negative to positive (i.e., I_j rectification is in the same direction as we found experimentally). When the charge is negative (Fig. 10 A, closed circle), rectification of the I_j-V_j plot is opposite in direction. The degree of rectification is lower when the charge is located closer to the center of the channel. The solid line shows the I_j-V_j plot for the channel without charge (i.e., z = 0). These rudimentary evaluations simply show that the γ_{res} dependence on V_j observed with the fast gate closed can be induced by introducing a positive charge located closer to the cytoplasmic end of the hemichannel. This makes the gated channel preferentially selective for anions; Fig. 10 B (inset) shows the ratio of ionic fluxes for Cl^- and K^+.

To test whether this simple model explains our experimental data demonstrating I_j rectification dependence on ionic composition, we used a charge profile (Fig. 10 C) consisting of positive charge at either cytoplasmic end, representing NH_2-terminal charges, and negative charge closer to the center representing charges in E1 or near the TM1/E1 border (Oh et al., 1999; Trexler et al., 2000). In symmetric KCl, this channel exhibits a linear I-V relation (Fig. 10 D, solid line) and nearly equal permeability to K^+ and Cl^+ (not shown). An increase in positive charge at one end, as a result of gating of one hemichannel to the substate, produces rectification such that current is larger when the side (hemichannel) that closes to the substate is made relatively negative (Fig. 10 D, dashed line). Narrowing of the pore was needed to substantially reduce the conductance. These data are plotted as the ratio $\gamma_{res}/\gamma_{open}$ in Fig. 10 E (solid line). By reducing the diffusion coefficient for the anion ~2.5-fold, to account for substitution of Asp^- for Cl^-, rectification is made slightly steeper (Fig. 10 E, dashed line). Conversely, reducing the diffusion coefficient for the cation the same amount reduces rectification (Fig. 10 E, dash-dot line). These changes in rectification are qualitatively similar to the experimental results, but considerably smaller in magnitude. Further reducing the diffusion coefficient of either the anion or cation could not explain the results. Closer agreement with the data could be obtained by assuming that the organic ions were permeant and exhibited binding in the channel (Fig. 10 F). The binding was modeled as a distributed negative (−0.2) or positive charge (+0.2) for Asp and TEA, respectively. Such binding is also consistent with the observed changes in open channel conductance upon substitution with either TEA or Asp; the magnitude of the reduction in either case was ~60%, greater than that expected by the reduced mobility of either the cationic or anionic component of the current, and suggestive of interactions within the channel that impede ionic fluxes. Although we did not attempt to replace both K and Cl, small but observable current flow through the residual state was reported in symmetric TEA-Asp salts, indicating these ions are permeable (Valiunas et al., 1997). Also, other studies have indicated that tetraalkylammonium ions and polyamines can display voltage-dependent block in homotypic Cx43 channels, which is consistent with their binding in the pore (Veenstra, 2001). Thus, our results suggest that the large changes in rectification upon substitution of larger organic ions can be explained by a combination of an electrostatic effect of the gating barrier and an electrostatic effect of the organic ions themselves permeating through the pore. We recognize that our model is rudimentary, and the assertion of a distributed charge contributed by binding of organic ions remains untested. More rigorous modeling will have to await more detail about the structure of the GJ channel pore.

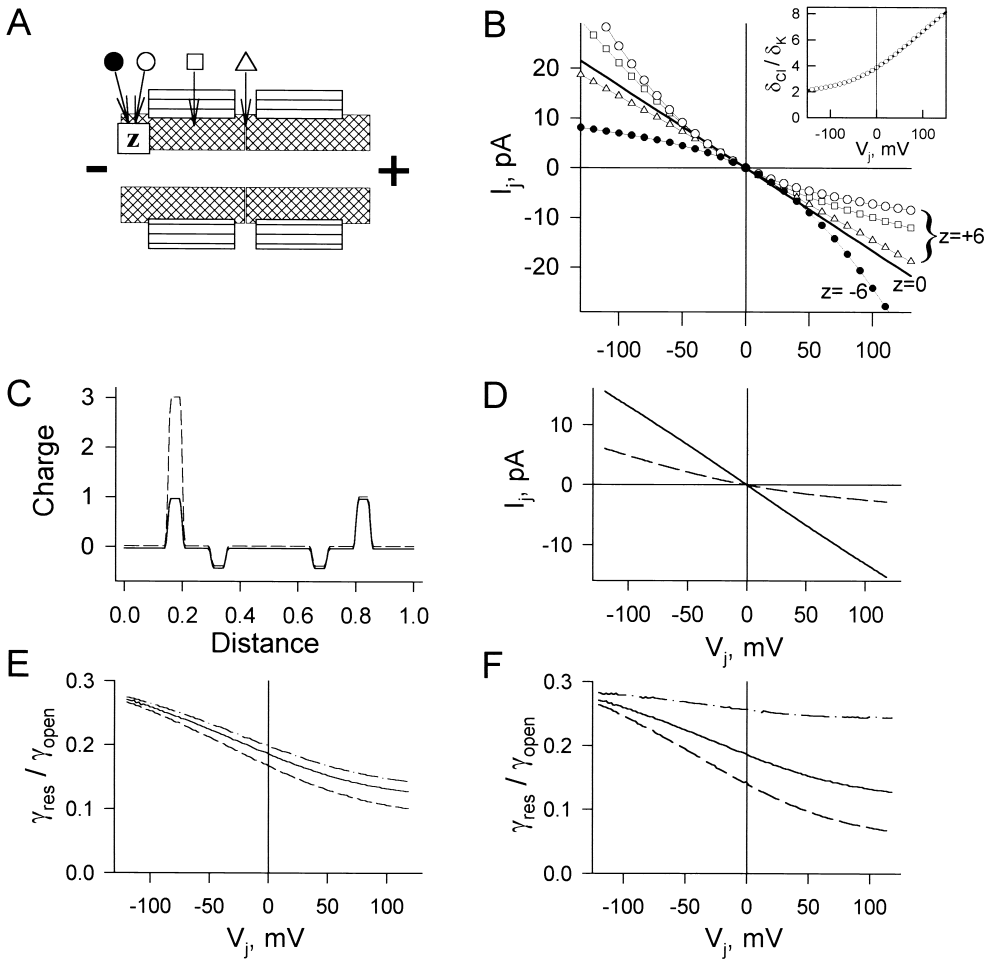

Figure 10. Introduction of positive charge at the cytoplasmic end of a gated Cx43 hemichannel can account for the current rectification that arises upon gating of a Cx43 channel to the residual state. (A) Schematic presentation of a channel pore as a cylinder 100 Å in length and 10 Å in diameter. The location of the charge introduced with gating is illustrated as a square, and z indicates the number of elementary charges. (B) PNP generated I-V curve for the channel in symmetric 140 mM KCl. Voltages are positive and negative relative to the gated side. Diffusion coefficients were 1.96×10^{-5} cm^2/s for K^+ and 2.03×10^{-5} cm^2/s for Cl^-. The solid line corresponds to z = 0. Curves with open symbols were generated with z = +6, one charge per subunit, located at different positions along the length of the pore; the symbols correspond to those indicated in A. The direction of I_j rectification is consistent with the experimental data and increases as the charge is moved toward the cytoplasmic end of the channel. The inset shows the ratio between fluxes for Cl^- and K^+ ions for the I-V curve indicated by open circles. The I-V curve with closed circles was generated with z = −6. (C) Charge profiles for a homotypic Cx43 channel. For the open channel (solid line), each hemichannel consists of positive charge located toward the cytoplasmic end and more centrally located negative charge (representing charges in at the M1/E1 border). Gating to the residual state is illustrated as an increase in positive charge in NT (dashed line). (D) PNP-generated I-V curves of open (solid line) and residual (dashed line) states for the charge profile shown in C. (E) PNP-generated plots of the ratio ($\gamma_{res}/\gamma_{open}$) calculated for the charge profile shown in C for a channel in symmetric KCl (solid line), KAsp (dashed line), and TEACl (dash-dot line). (F) The same as E, except that the charge profiles contained distributed positive or negative charge (z = ±0.2) corresponding to interaction of TEA and Asp, respectively, with the channel pore.

Dye transfer between cells generally has been used to evaluate whether there is diffusional cell–cell communication mediated by GJs. It is well established that open Cx43 channels are permeable to both mono- and divalent negatively and positively charged dyes, which is consistent with its poor charge selectivity (Larson et al., 1992; Steinberg et al., 1994; Veenstra et al., 1995; Elfgang et al., 1995, Bukauskas et al., 2000; Verselis et al., 2000). In addition, our unpublished data show that Cx43 channels are permeable to APTS (8-aminopyrene-1,3,6-trisulfonic acid, trisodium salt; MW = 523 D), which has three negative charges. Thus, Cx43 channels, like channels formed by many other members of the connexin gene family, form quite large pores. Examining cell–cell transfer of Alexa Fluor, we show that the high permeability characteristic of the open state is nearly abolished in the residual state. We devised an experimental procedure where we could examine dye transfer in the same cell pair under conditions in which the channels reside primarily in the open state or in the residual state. V_j steps were used to transfer the channel from the open to the residual state (Figs. 7 E and 8 C). Although we did not rigorously quantify permeability, it is clear from Fig. 7 D that intercellular flux of Alexa Fluor is reduced to a much greater extent in the residual state than predicted simply by the change in conductance. This occurs even with an increased preference for anions in the residual state and V_j gradient that favored dye transfer. Thus, it is likely that Alexa Fluor is impermeant in the residual state. The very small amount of flux observed is likely due to a small fraction of channels that occasionally gate to the open state. The

same conclusion is likely true for ethidium bromide, but transfer rates were low even in the open state. Several factors may be responsible for the difference in dye transfer of Alexa Fluor and ethidium bromide including the following: (1) Alexa Fluor remains free in the cytoplasm and does not bind to intracellular compounds, whereas ethidium bromide binds strongly to DNA, and its free concentration remains low until binding saturates; (2) fluorescence intensity of Alexa Fluor remains constant, whereas fluorescence intensity of ethidium bromide increases when it is bound to DNA.

In summary, rectification of a Cx43 channel closed to the residual state can be explained by the introduction of positive charge in the pore. With the knowledge that the Cx43 channel is gated from the side with negative V_j and the observation that γ_{res} decreases when V_j is made increasingly positive on the closed side, it would appear that the positive charge is most likely located close to the cytoplasmic vestibule of the gated hemichannel as proposed for Cx32 by Oh et al. (1999). In addition, gating to the residual state makes the Cx43 channel more anion-selective. Although the introduction of charge can explain the rectification, it cannot explain the reduced conductance of the gated channel, which is about five times smaller than that of the open state. Thus, the conformational change that results from gating to the residual state also leads to a significant narrowing of the channel pore that decreases channel conductance and reduces the cutoff size for permeant molecules. Our data indicate that molecules similar in size to fluorescent dyes (i.e., ~500 D) are excluded. Consequently, the V_j gating mechanism can serve as a selectivity filter that preserves electrical cell–cell communication but can limit the communication of metabolic or biological signaling molecules.

We would like to thank Dr. Laird for providing us Cx43-EGFP construct.

This study was supported by the National Institutes of Health grants NS36706 (to F.F. Bukauskas) and GM54179 (to V.K. Verselis).

Submitted: 8 November 2001
Revised: 31 December 2001
Accepted: 3 January 2002

REFERENCES

Banach, K., and R. Weingart. 2000. Voltage gating of Cx43 gap junction channels involves fast and slow current transitions. *Pflügers Arch.* 439:248–250.

Bennett, M.V., T.A. Bargiello, L. Barrio, D.C. Spray, E.L. Hertzberg, and J.C. Sáez. 1991. Gap junctions: new tools, new answers, new questions. *Neuron.* 6:305–320.

Bukauskas, F. 2001. Inducing de novo formation of gap junction channels. *In* Methods in Molecular Biology. Connexin: Methods and Protocols. Vol. 154. R. Bruzzone and C. Giaume, editors. Humana Press, Totowa, New Jersey. 379–393.

Bukauskas, F.F., and R. Weingart. 1994. Voltage-dependent gating of single gap junction channels in an insect cell line. *Biophys. J.* 67:613–625.

Bukauskas, F.F., and C. Peracchia. 1997. Two distinct gating mechanisms in gap junction channels: CO2-sensitive and voltage-sensitive. *Biophys. J.* 72:2137–2142.

Bukauskas, F.F., C. Kempf, and R. Weingart. 1992. Electrical coupling between cells of the insect *Aedes albopictus*. *J. Physiol.* 448:321–337.

Bukauskas, F.F., C. Elfgang, K. Willecke, and R. Weingart. 1995. Biophysical properties of gap junction channels formed by mouse connexin40 in induced pairs of transfected human HeLa cells. *Biophys. J.* 68:2289–2298.

Bukauskas, F.F., K. Jordan, A. Bukauskiene, M.V. Bennett, P.D. Lampe, D.W. Laird, and V.K. Verselis. 2000. Clustering of connexin 43-enhanced green fluorescent protein gap junction channels and functional coupling in living cells. *Proc. Natl. Acad. Sci. USA.* 97:2556–2561.

Bukauskas, F., A. Bukauskiene, M.V.L. Bennett, and V.K. Verselis. 2001. Gating properties of gap junction channels assembled from connexin43 and connexin43 fused with green fluorescent protein. *Biophys. J.* 81:137–152.

Chen, D.P., and R.S. Eisenberg. 1993. Flux, coupling, and selectivity in ionic channels of one conformation. *Biophys. J.* 65:727–746.

Elenes, S., A.D. Martinez, M. Delmar, E.C. Beyer, and A.P. Moreno. 2001. Heterotypic docking of Cx43 and Cx45 connexons blocks fast voltage gating of Cx43. *Biophys. J.* 81:1406–1418.

Elfgang, C., R. Eckert, H. Lichtenberg-Frate, A. Butterweck, O. Traub, R.A. Klein, D.F. Hulser, and K. Willecke. 1995. Specific permeability and selective formation of gap junction channels in connexin-transfected HeLa cells. *J. Cell Biol.* 129:805–817.

Falk, M.M. 2000. Connexin-specific distribution within gap junctions revealed in living cells. *J. Cell Sci.* 113:4109–4120.

Harris, A.L., D.C. Spray, and M.V. Bennett. 1981. Kinetic properties of a voltage-dependent junctional conductance. *J. Gen. Physiol.* 77:95–117.

Jordan, K., J.L. Solan, M. Dominguez, M. Sia, A. Hand, P.D. Lampe, and D.W. Laird. 1999. Trafficking, assembly, and function of a connexin43-green fluorescent protein chimera in live mammalian cells. *Mol. Biol. Cell.* 10:2033–2050.

Larson, D.M., R.J. Gilbert, and E.C. Beyer. 1992. Two-dimensional coupling by gap junctions in cultured gastric smooth muscle monolayers. *Am. J. Physiol.* 263:G261–G268.

Meyer, R.A., P.D. Lampe, B. Malewicz, W.J. Baumann, and R.G. Johnson. 1991. Enhanced gap junction formation with LDL and apolipoprotein B. *Exp. Cell. Res.* 196:72–81.

Moreno, A.P., M.B. Rook, G.I. Fishman, and D.C. Spray. 1994. Gap junction channels: distinct voltage-sensitive and -insensitive conductance states. *Biophys. J.* 67:113–119.

Moreno, A.P., E.C. Beyer, B.I. Fishman, and D.C. Spray. 1995. Voltage dependent gating and single channel analysis of heterotypic gap junction channels formed of Cx45 and Cx43. *In* Intercellular Communication through Gap Junctions Progress in Cell Research. Vol. 4. Y. Kanno, K. Kataoka, Y. Shiba, and Y. Shibata, editors. Elsevier Science Publishing Co., New York. 405–408.

Neyton, J., and A. Trautmann. 1985. Single-channel currents of an intercellular junction. *Nature.* 317:331–335.

Oh, S., J.B. Rubin, M.V. Bennett, V.K. Verselis, and T.A. Bargiello. 1999. Molecular determinants of electrical rectification of single channel conductance in gap junctions formed by connexins 26 and 32. *J. Gen. Physiol.* 114:339–364.

Oh, S., C.K. Abrams, V.K. Verselis, and T.A. Bargiello. 2000. Stoichiometry of transjunctional voltage-gating polarity reversal by a negative charge substitution in the amino terminus of a connexin32 chimera. *J. Gen. Physiol.* 116:13–31.

Peracchia, C. 1977. Gap junctions. Structural changes after uncoupling procedures. *J. Cell Biol.* 72:628–641.

Phelan, P., and T.A. Starich. 2001. Innexins get into the gap. *Bioessays.* 23:388–396.

Revel, J.P., and M.J. Karnovsky. 1967. Hexagonal array of subunits in intercellular junctions of the mouse heart and liver. *J. Cell Biol.* 33:C7–C12.

Revilla, A., C. Castro, and L.C. Barrio. 1999. Molecular dissection of transjunctional voltage dependence in the connexin-32 and connexin-43 junctions. *Biophys. J.* 77:1374–1383.

Ri, Y., J.A. Ballesteros, C.K. Abrams, S. Oh, V.K. Verselis, H. Weinstein, and T.A. Bargiello. 1999. The role of a conserved proline residue in mediating conformational changes associated with voltage gating of Cx32 gap junctions. *Biophys. J.* 76:2887–2898.

Rook, M.B., A.C. van Ginneken, B. de Jonge, A. el Aoumari, D. Gros, and H.J. Jongsma. 1992. Differences in gap junction channels between cardiac myocytes, fibroblasts, and heterologous pairs. *Am. J. Physiol.* 263:C959–C977.

Steinberg, T.H., R. Civitelli, S.T. Geist, A.J. Robertson, E. Hick, R.D. Veenstra, H.Z. Wang, P.M. Warlow, E.M. Westphale, J.G. Laing, and E.C. Beyer. 1994. Connexin43 and connexin45 form gap junctions with different molecular permeabilities in osteoblastic cells. *EMBO J.* 13:744–750.

Steiner, E., and L. Ebihara. 1996. Functional characterization of canine connexin45. *J. Membr. Biol.* 150:153–161.

Trexler, E.B., M.V. Bennett, T.A. Bargiello, and V.K. Verselis. 1996. Voltage gating and permeation in a gap junction hemichannel. *Proc. Natl. Acad. Sci. USA.* 93:5836–5841.

Trexler, E.B., F.F. Bukauskas, J. Kronengold, T.A. Bargiello, and V.K. Verselis. 2000. The first extracellular loop domain is a major determinant of charge selectivity in connexin46 channels. *Biophys. J.* 79:3036–3051.

Unwin, P.N.T., and G. Zampighi. 1980. Structure of the junction between communicating cells. *Nature.* 283:545–549.

Valiunas, V., F.F. Bukauskas, and R. Weingart. 1997. Conductances and selective permeability of connexin43 gap junction channels examined in neonatal rat heart cells. *Circ. Res.* 80:708–719.

Veenstra, R.D. 2001. Determining ionic permeabilities of gap junction channels. *Methods Mol. Biol.* 154:293–311.

Veenstra, R.D., H.Z. Wang, D.A. Beblo, M.G. Chilton, A.L. Harris, E.C. Beyer, and P.R. Brink. 1995. Selectivity of connexin-specific gap junctions does not correlate with channel conductance. *Circ. Res.* 77:1156–1165.

Verselis, V.K., M.V.L. Bennett, and T.A. Bargiello. 1991. A voltage-dependent gap junction in *Drosophila melanogaster. Biophys. J.* 59: 114–126.

Verselis, V.K., C.S. Ginter, and T.A. Bargiello. 1994. Opposite voltage gating polarities of two closely related connexins. *Nature.* 368:348–351.

Verselis, V.K., E.B. Trexler, and F.F. Bukauskas. 2000. Connexin hemichannels and cell-cell channels: comparison of properties. *Braz. J. Med. Biol. Res.* 33:379–389.

Weingart, R., and F.F. Bukauskas. 1993. Gap junction channels of insects exhibit a residual conductance. *Pflügers Arch.* 424:192–194.

Werner, R., E. Levine, E.C. Rabadan-Diehl, and G. Dahl. 1989. Formation of hybrid cell-cell channels. *Proc. Natl. Acad. Sci. USA.* 86: 5380–5384.

White, T.W., D.L. Paul, D.A. Goodenough, and R. Bruzzone. 1995. Functional analysis of selective interactions among rodent connexins. *Mol. Biol. Cell.* 6:459–470.

Willecke, K., D. Hennemann, E. Dahl, S. Jungbluth, and R. Heynkes. 1991. The diversity of connexin genes encoding gap junctional proteins. *Eur. J. Cell Biol.* 56:1–7.

Yeager, M. 1998. Structure of cardiac gap junction intercellular channels. *J. Struct. Biol.* 121:231–245.

Yeager, M., and B.J. Nicholson. 1996. Structure of gap junction intercellular channels. *Curr. Opin. Struct. Biol.* 6:183–192.